High-yield ligation-free assembly of DNA constructs with nucleosome positioning sequence repeats for single-molecule manipulation assays

Yi-Yun Lin[1,2], Tine Brouns[1,3], Pauline J. Kolbeck[1,2], Willem Vanderlinden[1,2,*], and Jan Lipfert[1,2,*]

From the [1]Department of Physics and Center for NanoScience (CeNS), LMU Munich, Munich, Germany; [2]Soft Condensed Matter and Biophysics, Department of Physics and Debye Institute for Nanomaterials Science, Utrecht University, Utrecht, The Netherlands; [3]Division of Molecular Imaging and Photonics, KU Leuven, Leuven, Belgium

Reviewed by members of the JBC Editorial Board. Edited by Craig Cameron

Force and torque spectroscopy have provided unprecedented insights into the mechanical properties, conformational transitions, and dynamics of DNA and DNA–protein complexes, notably nucleosomes. Reliable single-molecule manipulation measurements require, however, specific and stable attachment chemistries to tether the molecules of interest. Here, we present a functionalization strategy for DNA that enables high-yield production of constructs for torsionally constrained and very stable attachment. The method is based on two subsequent PCRs: first ∼380 bp long DNA strands are generated that contain multiple labels, which are used as "megaprimers" in a second PCR to generate ∼kbp long double-stranded DNA constructs with multiple labels at the respective ends. To achieve high-force stability, we use dibenzocyclooctyne-based click chemistry for covalent attachment to the surface and biotin–streptavidin coupling to the bead. The resulting tethers are torsionally constrained and extremely stable under load, with an average lifetime of 70 ± 3 h at 45 pN. The high yield of the approach enables nucleosome reconstitution by salt dialysis on the functionalized DNA, and we demonstrate proof-of-concept measurements on nucleosome assembly statistics and inner turn unwrapping under force. We anticipate that our approach will facilitate a range of studies of DNA interactions and nucleoprotein complexes under forces and torques.

DNA is central to the storage and transmission of genetic information. Single-molecule manipulation methods have provided unprecedented insights into the mechanical properties of DNA and its interaction with DNA-processing enzymes (1–10). Single-molecule force and torque spectroscopy experiments, in particular using optical or magnetic tweezers, require DNA constructs that are labeled at both ends with appropriate molecular handles to enable attachment to functionalized particles and surfaces (11, 12). Especially for torque and twist measurements, the requirements for molecular constructs are stringent, since torsional constraint requires multiple attachment sites at both ends and completely nick-free DNA, since a single nick removes the torsional constraint by enabling free rotation.

Preparation of DNA constructs with multiple attachment sites for single-molecule torque and twist assays requires several biochemical reactions. The most frequently used protocol involves PCR, restriction reactions, and final ligation to assemble three different DNA fragments into the final construct (4, 11, 13, 14). The central segment of the DNA molecule is unlabeled, whereas the two ends of the molecular construct are labeled with different moieties that enable attachment, with multiple biotin and digoxigenin (dig) labels, respectively, being a popular choice. The products of the ligation reactions are a mixture involving off-target DNA and unligated strands. Therefore, subsequent gel purification is often required to obtain the specific DNA construct. Unfortunately, these procedures lead to low yield and are prone to introduce nicks into the DNA.

To overcome the inefficiency of generating DNA through ligation-based protocols, improved methods are needed to simplify the process and increase the yield. Recently, new methods have been developed to generate high-yield DNA constructs for force and torque spectroscopy experiments (15). In particular, a ligation-free method has been reported that achieves high yield of torsionally constrained DNA and efficiently incorporates different labels at the end of DNA (16). The strategy is based on two PCR-synthesized DNA constructs that are used as "megaprimers" with biotin and dig labels, respectively, to amplify the target DNA in a final PCR step. The megaprimer-based PCR can create torsionally constrained DNA without ligation and restriction reactions. However, an additional requirement for biomechanical characterization at the single-molecule level is efficient and stable tethering of the biomolecules of interest. The commonly used attachment strategy relying on the binding of biotin to streptavidin-coated beads and the binding of dig-labeled nucleotides to a surface coated with antibodies against dig (anti-dig) is rapid and reliable. The biotin–streptavidin interaction exhibits good force stability, despite being noncovalent, and can be optimized through engineered streptavidin variants (17–19). Unfortunately, the antidig–dig interaction has much lower stability under forces >10 pN (20, 21). Therefore, it is desirable to go

* For correspondence: Willem Vanderlinden, W.Vanderlinden@uu.nl; Jan Lipfert, J.Lipfert@uu.nl.

beyond noncovalent attachment and introduce one or more covalent linkages, which can provide force stabilities up to nanonewton (22). Several approaches for covalent attachment have been developed (22–25) and provide stability for long measurements and experiments over a broad force spectrum (8, 26–30). For DNA attachment *via* dibenzocyclooctyne (DBCO), covalent binding to an azide-functionalized surface has been developed. This copper-free click chemistry method is specific, highly efficient, and yields tethers that are able to withstand very high forces (>100 pN) (25).

Here, we present a novel attachment protocol that combines the high yield enabled by the megaprimer approach with the supreme force stability afforded by covalent DBCO–azide coupling for anchoring DNA in tweezer experiments. Our strategy is based on DNA constructs with multiple biotin and DBCO labels at each end, respectively, and assembly *via* ligation-free PCR. The constructs enable torsionally constrained coupling and excellent force stability. The high yield of the approach enables us to obtain sufficient material for downstream biochemical preparation, in particular for nucleosome reconstitution.

The eukaryotic genome is highly compacted within the nucleus to form chromatin. Nucleosomes are the basic units of chromatin. Canonical nucleosome core particles are composed of two copies of H2A, H2B, H3, and H4 assembled into a histone octamer that is wrapped by 147 bp of DNA (31, 32). In order to study nucleosome interactions *in vitro*, nucleosome-positioning sequences with a high affinity for histone octamers are often used, and nucleosomes can be assembled by reconstitution, typically *via* salt dialysis. In particular, the "Widom 601" sequence (33) has become widely used for studies of nucleosome structure and function *in vitro*.

To reconstitute nucleosomes *in vitro*, at least 1 μg or 10 ng/μl DNA with appropriate positioning sequences (34–36) are required, to enable efficient handling and high enough concentrations for the assembly reaction. PCR amplifications of repetitive DNA and with megaprimers that contain different chemical labels are problematic as they can generate undesired products and low yield. Therefore, we optimized reaction conditions and tested different polymerases to obtain high yields. Finally, we characterized the mechanical properties of our new DNA constructs and the products of the nucleosome reconstitution. For both DNA and nucleosome constructs, we achieve reliable tethering and find mechanical signatures in good agreement with previous studies.

Results

Our protocol for the construction of end-labeled DNA constructs for single-molecule experiments has two key PCR steps (Fig. 1*A*). In the first step, regular primers are used in PCRs that include modified nucleotides to generate ~380 bp–labeled DNA constructs. These labeled DNA constructs are used as "megaprimers" in a second PCR with regular nucleotides to generate the final ~kbp DNA constructs with labeled ends.
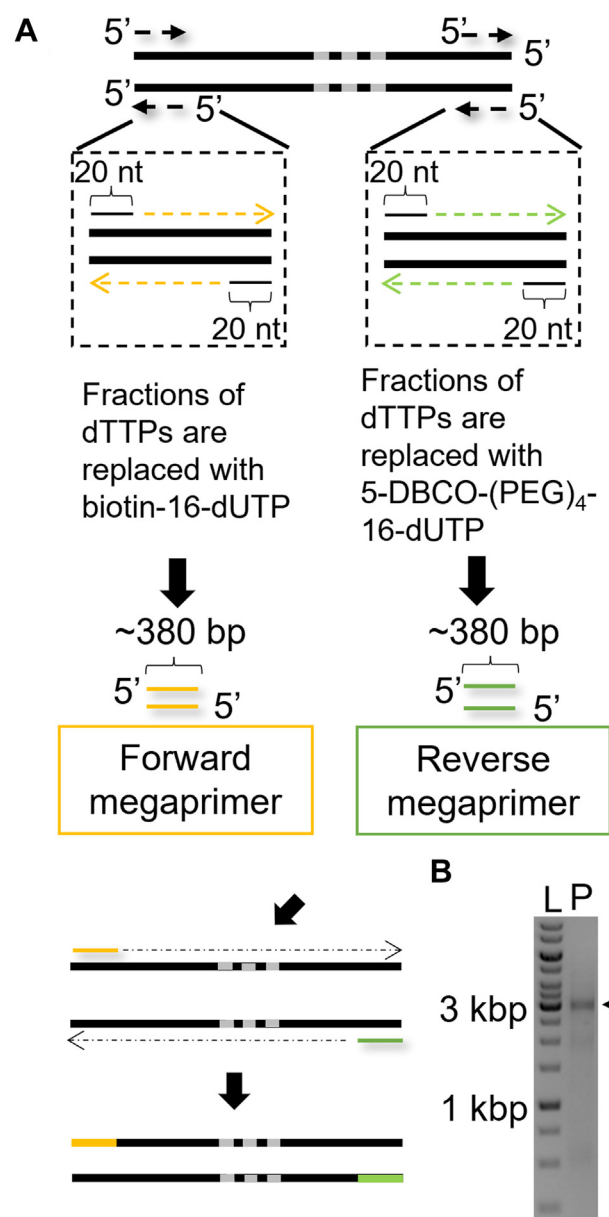
Figure 1. Ligation-free megaprimer PCR–based DNA assembly method. *A*, schematic of the ligation-free method to synthesize torsionally constrained DNA. Briefly, two sets of 20-nt ssDNA primers and linearized templates are used in PCRs to make two multilabeled ~380 bp DNAs that become the megaprimers. The two megaprimers are labeled with biotin and DBCO, respectively. A linearized template with three repeats of the Widom 601 sequence (shown schematically as *gray bars*) is used for subsequent PCR to get the final 2823 bp PCR construct. *B*, visualization of the PCR result by gel electrophoresis. The *left lane* ("L") has a DNA size ladder (1 kb PLUS; NE Biolabs). The *black arrow* in the *left lane* ("P") indicates the position of PCR product. DBCO, dibenzocyclooctyne.

Generation of labeled megaprimer constructs by PCR

We assembled 380 bp labeled megaprimer constructs by PCR. In the PCR to assemble functionalized megaprimers, we used 20 nt forward and reverse primers, pFMP218 as template, and a nonproofreading Taq polymerase or KOD Hot Start polymerase (Novagen; see the Experimental procedures section). We added biotin-16-dUTP or DBCO-(PEG)$_4$-dUTP to the PCR, up to 50% of modified dUTP. Gel analysis shows that the PCRs with labeled nucleotides yield single bands (Fig. S1).

As the percentage of modified dNTPs increases, a decrease in amplicon mobility is observed. This is consistent with the previously observed change in mobility because of the bulky side chains introduced by biotin-dUTP derivatives (37). We similarly attribute the mobility shift of the DBCO-(PEG)$_4$-dUTP substitution to the bulky side chain. We find that amongst the tested conditions, the mobility of the amplicons is lowest (and thus the number of incorporated labels the highest) for KOD Hot Start polymerase with 50% dTTP substitution (Fig. S1). We, therefore, use the megaprimers generated using the combination of KOD polymerase and 50% dTTP substitution in the subsequent steps.

Megaprimer PCR to generate labeled DNA constructs for single-molecule measurements

The megaprimer approach has originally been used for site-direct mutagenesis. More recently, the approach has been expanded by using biotin-labeled and dig-labeled megaprimers to generate DNA constructs with multiple labels at both ends by PCR amplification (16). We optimized conditions to assemble labeled DNA construct with arrays of nucleosome positioning sequences by PCR. A biotin-labeled megaprimer is used in this second PCR step as the forward primer, and a DBCO-labeled megaprimer is used as the reverse primer, to generate final DNA constructs with functionalized ends (Fig. 1A). To suppress off-target products, we prepared a linear template by PCR amplification. As the template, we used a 2823 bp plasmid DNA comprising three Widom 601 sequences. We followed the megaprimer method described previously (16) as a starting point, which uses KOD Hot Start polymerase, which is thermostable and designed to amplify difficult amplicons. We optimized PCR conditions by adding dimethyl sulfoxide (DMSO; New England Biolabs) and decreasing the polymerase concentration (Figs. S2 and S3 and Experimental procedures section). To test the applicability of the customized protocol, we combined different substitutions of megaprimers to process PCR. In our final protocol, we used megaprimers prepared with 50% biotin-dUTP and 50% DBCO-dUTP substitution (Fig. S2).

To test the reproducibility of our protocol, we performed five repeats of the PCR amplification for different megaprimer combinations. We find that each repeat of the experiments successfully amplified the target products (Fig. S2). To assess the purity from the PCR amplifications, we quantified the target product intensity relative to the integrated lane intensity (Fig. S2). The average purities from different combinations of megaprimers show similar values for different megaprimers used and are >50% in all cases tested. In summary, our optimized megaprimer PCR approach enables reproducible amplification of high-purity DNA constructs with specific modifications at both ends. The yield and purity are considerably higher than what is achieved in previous ligation-based protocols, which is critical in particular for nucleosome assembly on the functionalized DNA. In addition to the DNA constructs with three Widom 601 nucleosome positioning sequences, we also generated a functionalized DNA construct

with one Widom 601 (Fig. S4) and a longer 6.6 kbp DNA without nucleosome positioning sequences (Fig. S5), using the megaprimer approach with biotin and DBCO labels. In both cases, we obtained torsionally constrained DNA tethers suitable for magnetic tweezer experiments (Figs. S4 and S5), demonstrating the versatility of the approach.

Force response of megaprimer DNA constructs in magnetic tweezers

To obtain a high density of labels on the DNA, we use 50% biotin-dUTP and 50% DBCO-dUTP megaprimers for amplification and test the resulting labeled DNA construct in our single-molecule magnetic tweezer set up (Fig. 2A and Experimental procedures section). In the magnetic tweezer flow cell, the 2823 bp DNA tethers are anchored with copper-free click chemistry (25) to the surface and *via* biotin–streptavidin coupling to magnetic beads. We track the position of the magnetic beads while applying calibrated forces (38, 39). From the mean extension as a function of applied force, we obtained force–extension curves (Fig. 2B). As expected, the force–extension behavior of DNA closely follows the extensible worm-like chain model until ∼40 pN. At forces >60 pN, the force–extension response of the DNA tethers exhibits two different behaviors: some molecules still behave similar to the worm-like chain model, whereas others exhibit overstretching behavior at about 65 pN, which corresponds to the characteristic signature of stretching torsionally unconstrained double-stranded DNA (2, 40, 41). The absence of an overstretching transition in our force range for some DNA tethers is consistent with the expectation for fully torsionally constrained DNA, for which the overstretching transition is suppressed at forces below 110 pN (2, 41).

To determine the lifetime of our DNA tethers under mechanical load, we subjected them to a constant force of 45 pN and recorded the position traces of the beads until rupture of the molecular tethers. We analyzed the lifetimes until rupture and find an approximately exponential lifetime distribution with a fitted mean lifetime of 70 ± 3 h (Fig. 2C). Our DNA construct is modified with multiple biotin and DBCO labels at the opposite ends. The DBCO-based coupling has been reported to provide force stability up to nanonewton (22, 25). In contrast, while the streptavidin–biotin bond has an extraordinarily high affinity ($K_d \sim 10^{-14}$ M), the interaction is noncovalent and can be broken under external forces well below 1 nN (17, 19, 42). The tetrameric structure of streptavidin and its nonspecific coupling for commercially available beads means that different force-loading geometries are possible, which gives rise to a broad range of multiexponential lifetimes (17–19). Previous work has shown that an engineered monovalent variant of streptavidin in the most stable geometry (1SA) exhibits a lifetime $\tau_1 = 11.2 \pm 0.4$ h at 45 pN for a single biotin–streptavidin bond. We attribute the fact that we observe an even longer lifetime than what was found for the single engineered streptavidin at the same force, despite using commercially available beads without the optimized streptavidin, to the fact that our tethers feature multiple biotin labels

Megaprimer assembly of DNA tethers for force spectroscopy
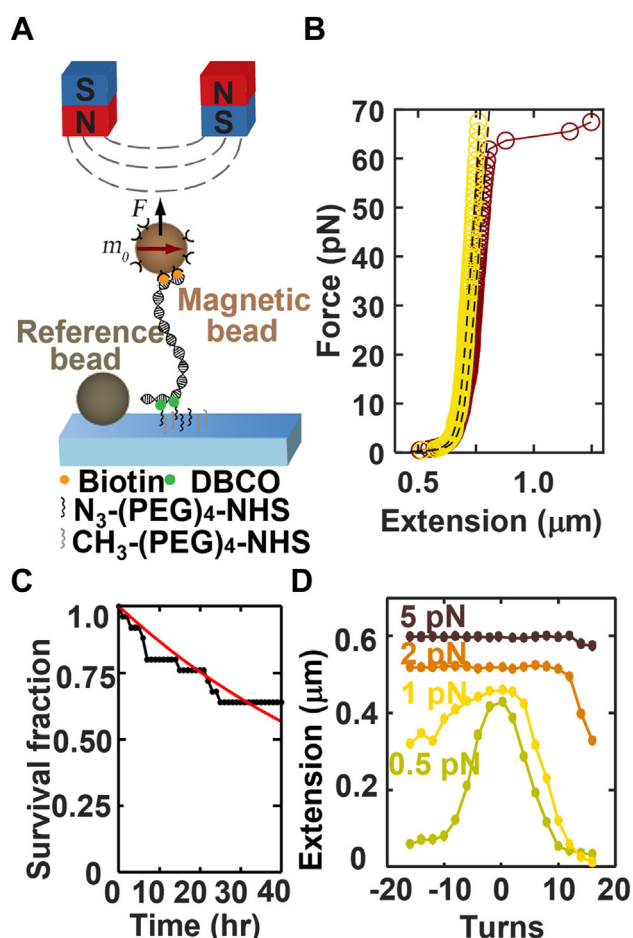
Figure 2. Force spectroscopy experiments on megaprimer-generated DNA constructs in magnetic tweezers. *A*, schematic of the magnetic tweezer set-up. The flow cell surface is functionalized with azide-(PEG)$_4$-NHS. The DNA construct has two handles, one labeled with multiple biotins and the other with multiple DBCOs. The biotins bind to multiple streptavidins that coat the magnetic bead and DBCOs at the other end form the covalent bond with the azide group. *B*, force–extension curves of DNA molecules anchored as shown in *A*. Representative force–extension measurements of torsionally constrained (*yellow*), unconstrained DNA molecules (*brown*), and coplot of the extensible worm-like chain (WLC) model with a bending persistence length of 45 nm (*black dashed line*). Torsionally unconstrained DNA exhibits the overstretching transition near 65 pN; the torsionally constrained molecule does not overstretch at 65 pN. *C*, fraction of DNA tethers remaining as a function of time when subjected to a constant force of 45 pN. The *red line* is an exponential fit to the data with a mean lifetime of (70 ± 3) h. Analyzing the torsionally constrained and unconstrained tethers separately, we find very similar lifetimes of 68 ± 2 h and 76 ± 3 h. *D*, extension–rotation curves at constant forces of 0.5, 1, 2, and 5 pN indicate that the DNA construct is torsionally constrained and shows the well-known response of double-stranded DNA (4, 5). DBCO, dibenzocyclooctyne.

that can bind to the bead and, therefore, significantly increase the overall lifetime under force. Similarly, Janissen *et al.* (21) have investigated different DNA constructs by using magnetic tweezers. They found that the lifetime under a force of 45 pN for traditional biotin and dig-based DNA anchoring is only ∼7 min. If the dig is replaced by covalent anchoring while retaining the single biotin–streptavidin linkage at the other end, the lifetime increases to ∼3 h, highlighting the dramatic increase in force stability afforded by replacing the dig–antidig coupling to the surface with a covalent attachment approach. The fact that we achieve an approximately 20-fold longer

lifetime compared with Janissen *et al.* might be due to their lower label density or the fact that they used neutravidin instead of streptavidin (13, 21).

Torsional response of megaprimer DNA constructs in magnetic tweezers

To determine whether our attachment protocol with multiple labels at both ends enables supercoiling experiments on DNA tethers, we systematically underwound and overwound the DNA by rotating the magnets from −16 to 16 turns at forces of 0.5, 1, 2, and 5 pN (Fig. 2*D*). Below 1 pN, the rotation curve of DNA behaves symmetrically and the extension of DNA decreases on overwinding or underwinding past the buckling point (4, 5, 13). At 1 and 2 pN, the extension–rotation response of the DNA is asymmetric, because of torque-induced melting of the DNA (43). Overall, our measurements recapitulate the well-known extension–rotation response of double-stranded DNA. We typically obtain 50% of supercoilable (*i.e.*, fully torsionally constrained) DNA tethers (27 of 57 tethers), comparable to previous protocols (15, 16). For the 6.6 kbp DNA construct without nucleosome positioning sequences, we performed additional experiments using high-speed tracking at 1 kHz and recapitulate also the known behavior of the variance of the extension fluctuations upon overwinding and underwinding (44) (Fig. S5, *C* and *D*).

Estimation of labeling efficiency from magnetic tweezers ruptures time traces

Examining the extension time traces prior to tether rupture carefully, we find occasional steps in the tether extension (Fig. 3*A*). Increases in tether extension prior to tether rupture are consistent with the disruption of biotin–streptavidin bonds, where the final rupture corresponds to the last biotin–streptavidin pair. We quantified the observed steps and find a rather broad distribution with a mean step size of 13.0 nm ± 14.8 nm (mean ± standard deviation). We then compared the experimental step size distributions (Fig. 3*B*, *gray bars*) to a simple model for step sizes based on the experimentally used megaprimer sequences and simulated label incorporation (see the section "Model for the step size distributions" in the Experimental procedures section). Our simple model can account for the overall shape of the observed step size distribution, with an initial sharp increase and subsequent slow decay of the probability of steps with their size. The predicted step size distribution shifts to smaller step sizes for higher label efficiencies P_{label} (Fig. 3*B*, *colored lines*), where P_{label} represents a combined effective probability of incorporating a label and binding to an available streptavidin. We find good agreement both of the mean step size and overall distribution (Fig. 3, *C* and *D*) for P_{label} = 0.1. The best fitting value of P_{label} = 0.1 is fivefold lower than the ratio of labeled nucleotides in the PCR mix (which is 50%), which suggests that the KOD polymerase used in our experiments preferentially incorporates unlabeled nucleotides, similar to what has been reported for other polymerases (45–50) and/or that not all incorporated biotin labels attach to a streptavidin-binding site,
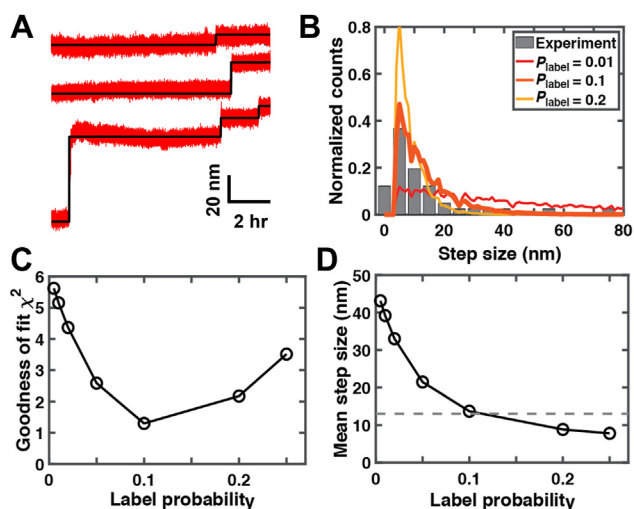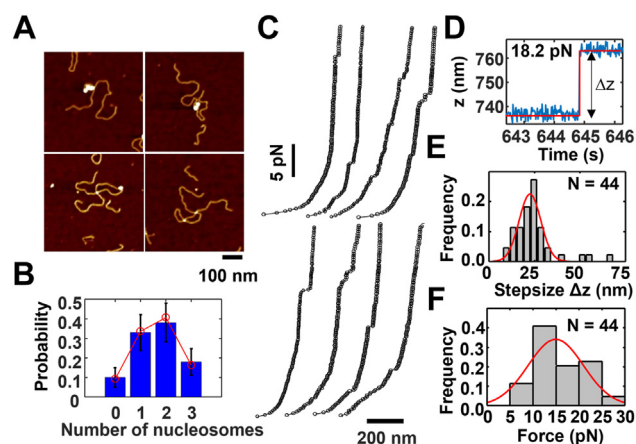
Figure 3. Analysis of tether rupture steps to estimate the labeling efficiency for DNA tethers. *A*, examples of the rupture steps in extension time traces under an applied force of 45 pN (*red lines*). The *black lines* are steps in the traces as determined by a step finding algorithm (63). *B*, experimentally observed step sizes in extension time traces before tether dissociation (*gray bars*; N = 41 steps). Coplotted are the step size distribution predicted by our simple model (see "Model for the step size distributions" in the Experimental procedures section) that takes into account stochastic label incorporation for three selected values of the label probability P_{label} (*color lines*; P_{label} values are indicated in the legend; simulation results are for 100,000 simulated tethers for each condition). *C*, goodness of fit comparing simulated step size distribution with the experimental data. The goodness of fit is computed as the sum of squared differences of normalized counts in each bin for simulated and experimentally observed data. *D*, mean step size from simulated step size distributions *versus* P_{label}. The *horizontal dashed line* corresponds to the experimentally determined value. Standard errors of the mean are not shown, as they are smaller than symbol sizes.

Figure 4. Nucleosome constructs for magnetic tweezer measurements. *A*, atomic force microscopy (AFM) images of megaprimer PCR generated DNA after nucleosome reconstitution. Images show DNA constructs with 3, 2, 1, or no nucleosomes assembled (*left* to *right*, *top* to *bottom*). *B*, histogram of the number of nucleosomes assembled on the DNA constructs obtained from AFM images (N = 39 DNA molecules; error bars are from counting statistics). *Red points* are the best fit of a binomial distribution with fitted assembly probability p = 0.55. *C*, force–extension curves of polynucleosome DNA constructs from 0.5 to 30 pN. The *traces* show different length plateaus at forces ≤7 pN that indicate outer turn unwrapping and unstacking of polynucleosomes. At higher forces (>7 pN), we observe discrete steps in extension that represent the full unwrapping of polynucleosomes. *D*, example of a discrete step in time traces at forces >7 pN, characteristic of the unwrapping of the inner DNA turn from nucleosomes (raw data in *blue*; the fitted step is shown in *red*). *E*, histogram of the step sizes for inner turn unwrapping. The *red line* is Gaussian fit, indicating a step size of 22.6 ± 5.9 nm (mean ± standard deviation). *F*, histogram of the forces for inner turn unwrapping. The average rupture force is 16 ± 6 pN (mean ± standard deviation).

likely because of steric constraints. These observations are also consistent with the finding that, while in principle torsionally constrained attachment of DNA or RNA tethers only requires two attachment sites at each end, in practice at least ~10 potential attachment sites should be incorporated at the respective ends to ensure a high number of stable and torsionally constrained tethers (40).

Assembly of nucleosomes for magnetic tweezer experiments

To test whether our megaprimer assembly-based DNA construct can be used to assemble and measure nucleosomes, we carried out nucleosome reconstitution *via* salt gradient dialysis to obtain polynucleosomes (see the Experimental procedures section). We used atomic force microscopy (AFM) imaging to confirm the assembly of nucleosomes and quantified the different polynucleosome populations, by counting the number of mononucleosomes, dinucleosomes, and trinucleosomes that are successfully assembled (Fig. 4*A*). The populations for bare DNA, and DNA with one, two, and three nucleosomes, are consistent, within experimental errors, with a simple binomial distribution (Fig. 4*B*), which implies that nucleosome assembly on the three Widom 601 sites is relatively uncooperative under the conditions of our experiments, consistent with previous observations (51).

To measure the nucleosomes in the magnetic tweezers, the nucleosome constructs are tethered between the bottom surface of a flow cell and a superparamagnetic bead using the same coupling approach that we use for bare DNA (Fig. 2*A*). We performed force–extension experiments on the nucleosome tethers by systematically increasing the force from 0.5 to 30 pN in 0.2 pN increments and recording time traces at each force for 5 s (Fig. 4*C*). The extension traces exhibit small and variable steps in the force region between 2 and 7 pN, which we attribute to unwrapping of the outer turn of DNA from nucleosomes and the disruption of nucleosome–nucleosome interaction. At forces >7 pN, larger and more uniform steps are observed, in agreement with previous reports (36, 52–62) of unwrapping of the inner turn of nucleosomes (Fig. 4, *C* and *D*). We quantified the high-force steps by employing the step finding algorithm by Kerssemakers *et al.* (63) to identify unwrapping steps in our extension *versus* time traces (Fig. 3*D*) and to determine the differences between average extensions before and after the steps to obtain step sizes. The distribution of step sizes shows a clear peak at 22.6 ± 5.9 nm (mean ± standard deviation; Fig. 4*E*), in good agreement with previous reports for step sizes of inner turn nucleosome unwrapping in the range of 20 to 30 nm (36, 52–62). We observe the inner turn unwrapping steps over a relatively broad range of forces, with a mean ± standard deviation of 16 ± 6 pN (Fig. 4*F*). Previously reported values of the force at which inner turn unwrapping occurs depend on a range of factors, including force loading rate, ionic strength, and the nucleosomal positioning element (1, 52–54, 57, 59–61). Previous work using a

similar ionic strength and the Widom 601 sequence ([59], [60]) found inner turn unwrapping between 7 and 40 pN, using constant loading rate measurements. For constant force measurements, it was reported that the lifetime at 7 pN is similar to 10 s and then decreases to 1 s at force ≥10 pN ([64]), consistent with our experimental findings.

Discussion

In summary, we present a new method for preparing functionalized DNA constructs for single-molecule measurements that combines the benefits of ligation-free high-yield megaprimer-based assembly and covalent attachment of DNA to the surface for very high-force stability. Our tethers are torsionally constrained and thus enable torque and twist measurements. In addition, they provide exceptionally high-force stability, and we find an average lifetime of (70 ± 3) h at 45 pN using regular, commercially available streptavidin-coated beads. The high yield of correctly labeled DNA enables efficient nucleosome reconstitution by standard salt gradient dialysis, and we demonstrate proof-of-concept measurements on nucleosome assembly quantified by AFM imaging and disassembly under external forces in magnetic tweezers. We anticipate that our methodology will enable a range of measurements on DNA and nucleoprotein complexes that benefit from high yield and force stability.

Experimental procedures

DNA preparation

We used the plasmid pFMP218 ([65]) as template to produce DNA constructs with nucleosome positing sequences. pFMP218 is a custom-built plasmid (provided by Prof. Felix Müller-Planitz, TU Dresden) from a pUC18 backbone and with three repeats of the Widom 601 sequence inserted. The final design yields a 2823 bp DNA molecule with a 2055 bp central unlabeled segment, flanked by two ~380 bp labeled regions. We generated the 2823 bp DNA construct from pFMP218 as linear template for subsequent assembly by PCR with Phusion Hot Start polymerase (follow the vendor's protocol) using forward primer 5′-GCAGAAGTGGTCCTGCAACT-3′ and reverse primer 5′-CCGGATCAAGAGCTACCAAC-3′.

Functionalized handles (the "megaprimers"; Fig. 1*A*) were obtained by PCR amplification. We tested both Taq polymerase (New England Biolabs) and KOD Hot Start polymerase to prepare the functionalized handles and found both to give good yields of functionalized DNA product (Fig. S1). For both polymerases, we ran PCR with added biotin-16-dUTP or 5-DBCO-(PEG)$_4$-dUTP (Jena Biosciences GmbH), respectively. For Taq polymerase, the PCR used 0.3 μM forward primer 5′-GCAGAAGTGGTCCTGCAACT-3′, 0.3 μM reverse primer 5′-CGCCGCATACACTATTCTCA-3′, 6 ng template DNA, and different amounts of biotin-16-dUTP (0.16, 0.08, or 0.04 mM final concentration) in 20 μl 1× Taq Master Mix (which contains a final concentration of 0.2 mM of each unmodified dNTP). The other PCR solution contains 0.3 μM forward primer 5′-CCGCTTACCGGATACCTGTC-3′, 0.3 μM reverse primer 5′-

CCGGATCAAGAGCTACCAAC-3′, 6 ng template DNA, and different amounts of 5-DBCO-(PEG)$_4$-dUTP (0.16, 0.08, or 0.04 mM final concentration) in 20 μl 1× Taq Master Mix.

For KOD Hot Start polymerase, we followed a previous protocol ([16]). We used the same DNA template and primers as for Taq polymerase and incorporated labeled dUTPs by replacing dTTPs in the PCR mix ([66]) using either 25% or 50% biotin-16-dUTP or DBCO-(PEG)$_4$-dUTP (the final concentrations are 0.05/0.15 and 0.1/0.1 mM modified dUTP/unmodified dTTP), respectively.

The functionalized PCR products are subsequently used as megaprimers to amplify the desired DNA substrate. We used KOD Hot Start polymerase for this PCR. Instead of following the vendor's protocol, we changed the reaction conditions to optimize the purity and yield of our target DNA (Fig. S2). Our final protocol uses KOD Hot Start polymerase with a reaction solution containing 1.5 mM MgCl$_2$, 0.16 mM × 4 dNTP, 1× KOD Hot start buffer, 7.5% DMSO, 200 ng forward megaprimer, 200 ng reverse megaprimer, 50 ng linear template from pFMP218, and 0.5 μl (1 unit/μl) KOD Hot start polymerase in 100 μl reaction volume. We used the following PCR cycling parameters: initial denaturation at 95 °C for 2 min; 35 cycles of denaturation at 95 °C for 20 s, annealing at 60 °C for 10 s, and elongation at 70 °C for 65 s. The final cycle was followed by extension at 70 °C for 1 min. The PCR products were purified with the QIAquick PCR Purification Kit (Qiagen) after each step of PCR amplification. One reaction with a final volume of 100 μl typically produces 0.6 μg DNA, of which approximately 70% is the correctly assembled megaprimer DNA (Fig. S2*E*). This amount of product is similar to a previously described megaprimer protocol using dig labeling ([16]) and significantly higher than previous non-PCR–based protocols ([13], [15]).

We also tested PCRs using a 5× smaller reaction volume and 5× higher final concentrations of megaprimers and template DNA, using 10% DMSO and 1× KOD Hot start polymerase MasterMix (Fig. S3). The smaller final volume facilitates downstream processing, and the higher megaprimer concentration has been suggested to increase yield ([67], [68]). While the PCRs at higher concentrations yield functionalized DNA constructs, we find more off-target products (Fig. S3) and greater variability in yield. Therefore, we recommend the reaction described previously with a final reaction volume of 100 μl.

Nucleosome reconstitution

Nucleosomes were assembled on the labeled DNA construct obtained using the megaprimer protocol outlined in the previous section. Recombinant human histone octamers were purchased from EpiCypher. Samples were prepared *via* salt gradient dialysis following the protocol described previously ([69]). In brief, 2.7 μg DNA (~150 nM of 601 motifs) and 0.6 μg histone octamer (170 nM) in 30 μl high-salt buffer (10 mM Tris–HCl, pH 7.6, 1 mM EDTA, 0.1% [w/v] Triton X-100, and 2 M NaCl) were incubated in a dialysis chamber (Slide-A-Lyzer MINI Dialysis Devices, 3.5 K molecular weight cutoff; Thermo Scientific) at 4 °C. Then, the dialysis chamber was

transferred to a glass beaker with 300 ml high-salt buffer and 300 µl β-mercaptoethanol. About 3 l low-salt buffer (10 mM Tris–HCl, pH 7.6, 1 mM EDTA, 0.1% [w/v] Triton X-100, and 50 mM NaCl) and 300 µl β-mercaptoethanol were transferred to the high-salt buffer overnight at 4 °C (at least 16 h). The buffer exchange was achieved with a peristaltic pump to slowly introduce the low-salt buffer into the beaker with the dialysis chamber. Finally, we placed the dialysis chamber into 1 l low-salt buffer with 300 µl β-mercaptoethanol for 1 to 2 h.

Magnetic tweezer setup

We used a custom-built magnetic tweezer setup described previously (70). The setup employs a pair of $5 \times 5 \times 5$ mm³ permanent magnets (W-05-N50-G; Supermagnete) with a 1 mm gap in vertical configuration (38). We used a DC motor (M-126.PD2, P1) to control the distance between magnets and the flow cell. An LED (69647; Lumitronix LED Technik GmbH) was used for illumination. We used a 40× oil-immersion objective (UPLFLN 40×; Olympus) and a CMOS sensor camera with 4096×3072 pixels (12M Falcon2; Teledyne DALSA) to image a field of view of 400×300 µm². Images were recorded at 58 Hz and transferred to a frame grabber (PCIe 1433; National Instruments). Images are tracked in real time with custom-written tracking software (Labview, National Instruments) to extract the (x, y, z) coordinates of all beads (71). The objective is mounted on a piezo stage (Pifoc P726. 1CD, PI Physikinstrumente) to build a look-up table for tracking the bead z-position. With a step size of 100 nm, the look-up table was generated over a range of 10 µm. Set up control and bead tracking used Labview routines described previously (71).

Flow cell assembly and preparation

Flow cells were assembled from two microscope cover slips with a parafilm spacer. The bottom coverslip (24×60 mm; Carl Roth) was treated with 2% APTES to generate an aminosilanized surface. Before flow cell assembly, 5000× diluted stock solution of polystyrene beads (Polysciences) in ethanol (Carl Roth) was deposited on the amino-coated coverslip and then slowly dried. These immobile surface-bound beads serve as reference beads for drift correction. The bottom coverslip was aligned with a precut parafilm and a top coverslip with two small holes for inlet and outlet. Then the assembled flow cell was baked at 80 °C for 1 min.

DNA or polynucleosome anchoring for magnetic tweezer experiments

Following flow cell assembly, 50 mM each of azide-(PEG)₄-NHS (Jena Biosciences GmbH) and methyl-(PEG)₄-NHS (Life Technologies) in 1× PBS were introduced and incubated for 1 h (25). To prepare the solution, 100 mg azide-(PEG)₄-NHS or methyl-(PEG)₄-NHS were dissolved in 100 µl DMSO, respectively, to prevent hydrolysis of the NHS ester during storage at −20 °C. We added 1× PBS buffer to adjust to a final concentration of 100 mM for both azide-(PEG)₄-NHS and methyl-(PEG)₄-NHS, respectively, and then mix equal volumes. The

mixture was quickly filled into the incubation chamber for surface passivation to avoid hydrolysis. We found that the addition of salt in Hepes buffer (10 mM Hepes, pH 7.6) is necessary to immobilize DNA or polynucleosomes on the surface of the flow cell. Therefore, we mixed our DNA or polynucleosome sample in measurement buffer MB1 (MB1; 10 mM Hepes [pH 7.6], 100 mM KCl, 2 mM MgCl₂, and 0.1% Tween-20). Next, the flow cell was flushed with 500 µl MB1. DNA or polynucleosomes were dissolved in 100 µl MB1, flushed into the flow cell, and incubated for 1 h. Afterward, we rinsed with MB2 buffer, which consists of MB1 supplemented with 0.1% (w/v) bovine serum albumin (Carl Roth). The flow cell was rinsed with MB2 to flush out unbound DNA or nucleosomes. Subsequently, we flowed in 1% casein for nucleosome samples or 1.5% (w/v) bovine serum albumin for DNA samples in MB2 into the flow cell, incubated for 1 h to minimize nonspecific interactions, and then flushed with MB2. Finally, we flushed in streptavidin-coated M270 beads (Dynabeads; Invitrogen) and incubated in the flow cell for 10 min. Subsequently, unbound beads were flushed out with 2 ml MB2.

AFM sample preparation, imaging, and analysis

We follow the previously published protocol to prepare samples for AFM imaging (72–75). Briefly, reconstituted nucleosomes were incubated in 200 mM NaCl and 10 mM Tris–HCl, pH 7.6, for 1 min on ice and then deposited on poly-L-lysine (0.01% w/v)–coated muscovite mica for 30 s, followed by 20 ml Milli-Q water rinsing, and drying with a gentle stream of filtered nitrogen gas. AFM imaging was performed on a Nanowizard Ultraspeed 2 (JPK) with AFM cantilevers, FASTSCAN-A (resonance frequency 1400 kHz, spring constant 18 N/m; Bruker) for high-speed imaging in air. All AFM images were acquired in tapping mode at room temperature. The scans were recorded at 3 Hz line frequency over a field of view of 3 µm × 3 µm at 2048 × 2048 pixels. For image processing, Scanning Probe Image Processor (SPIP, version 6.4; Image Metrology) was employed. Image processing involved background correction by using global fitting with a third-order polynomial and line-by-line correction through the histogram alignment routine.

Model for the step size distributions

When subjecting the megaprimer-DNA tethers to constant forces, we observe stepwise increases in the tether length prior to tether rupture. Here, we describe a simple and minimal model to account for the experimentally observed step size distribution. Since the covalent linkages used in our protocol are expected to be very force stable, we assume that only the biotin–streptavidin bonds dissociate under the constant loads exerted in the magnetic tweezer assay and cause the observed steps on the time scale of our experiments (17, 19). As a starting point, we used the DNA sequence for the biotin megaprimer assembly. In our reaction, a fraction of the thymidine moieties in the DNA sequence is replaced by biotinylated uridine. However, it is important to note that not all thymidine moieties in the sequence will form bonds to the magnetic bead since (i) the PCR contains a mix of labeled and

unlabeled nucleotides, (ii) the polymerase might incorporate labeled and unlabeled nucleotides with different probabilities (50, 76), (iii) not all labeled nucleotides will bind to a streptavidin on the bead because of steric constraints, amongst other reasons. We assume that the incorporation and subsequent binding to streptavidin of functionalized nucleotides are random and occurs with probability P_{label} that we treat as a fitting parameter. We used a Monte Carlo approach whereby PCRs are simulated by randomly incorporating labels at T positions in the sequence with probability P_{label}. To convert the simulated label positions in the sequence to step sizes, we further assumed that streptavidin can only bind labels that are at least 10 bp apart, corresponding to a minimal physical distance of ~3 nm, since it is unlikely that two streptavidin tetramers (77) would bind within one helical turn. Simulated step size distributions are obtained by converting the distances between subsequent incorporated and streptavidin-bound labels from basepair to nanometer using a conversion factor of 0.34 nm/bp, corresponding to the crystallographic length of double-stranded DNA. The experimentally determined step size distribution is compared with the experimental data using an unweighted χ^2 criterion. In addition, we compare the mean step sizes of the simulated and experimental data.

Data availability

All data are included in the article. Custom software written in MATLAB is available freely in the repository YODA at https://doi.org/10.24416/UU01-U63Z8W.

Author contributions—Y.-Y. L., T. B., W. V., and J. L. conceptualization; J. L. methodology; J. L. software; Y.-Y. L., T. B., and P. J. K. investigation; Y.-Y. L., P. J. K., and J. L. visualization; Y.-Y. L. writing–original draft; T. B., P. J. K., W. V., and J. L. writing–review & editing; W. V. and J. L. supervision; W. V. and J. L. project administration; J. L. funding acquisition.

References

1. Bustamante, C., Bryant, Z., and Smith, S. B. (2003) Ten years of tension: single-molecule DNA mechanics. *Nature* **421**, 423–427
2. Smith, S. B., Cui, Y., and Bustamante, C. (1996) Overstretching B-DNA: the elastic response of individual double-stranded and single-stranded DNA molecules. *Science* **271**, 795–799
3. Smith, S. B., Finzi, L., and Bustamante, C. (1992) Direct mechanical measurements of the elasticity of single DNA molecules by using magnetic beads. *Science* **258**, 1122–1126
4. Strick, T. R., Allemand, J. F., Bensimon, D., Bensimon, A., and Croquette, V. (1996) The elasticity of a single supercoiled DNA molecule. *Science* **271**, 1835–1837
5. Kriegel, F., Ermann, N., and Lipfert, J. (2017) Probing the mechanical properties, conformational changes, and interactions of nucleic acids with magnetic tweezers. *J. Struct. Biol.* **197**, 26–36
6. Bai, L., Santangelo, T. J., and Wang, M. D. (2006) Single-molecule analysis of RNA polymerase transcription. *Annu. Rev. Biophys. Biomol. Struct.* **35**, 343–360
7. Lipfert, J., van Oene, M. M., Lee, M., Pedaci, F., and Dekker, N. H. (2015) Torque spectroscopy for the study of rotary motion in biological systems. *Chem. Rev.* **115**, 1449–1474
8. Zhou, J., Schweikhard, V., and Block, S. M. (2013) Single-molecule studies of RNAPII elongation. *Biochim. Biophys. Acta* **1829**, 29–38
9. Meglio, A., Praly, E., Ding, F., Allemand, J. F., Bensimon, D., and Croquette, V. (2009) Single DNA/protein studies with magnetic traps. *Curr. Opin. Struct. Biol.* **19**, 615–622
10. Neuman, K. C. (2010) Single-molecule measurements of DNA topology and topoisomerases. *J. Biol. Chem.* **285**, 18967–18971
11. Vilfan, I. D., Lipfert, J., Koster, D. A., Lemay, S. G., and Dekker, N. H. (2009) Magnetic tweezers for single-molecule experiments. In: Hinterdorfer, P., Oijen, A., eds. *Handbook of Single-Molecule Biophysics*, Springer US, New York, NY: 371–395
12. Bryant, Z., Oberstrass, F. C., and Basu, A. (2012) Recent developments in single-molecule DNA mechanics. *Curr. Opin. Struct. Biol.* **22**, 304–312
13. Lipfert, J., Koster, D. A., Vilfan, I. D., Hage, S., and Dekker, N. H. (2009) Single-molecule magnetic tweezers studies of type IB topoisomerases. *Methods Mol. Biol.* **582**, 71–89
14. Clarke, D. J., and Lane, A. (2009) Introduction: emerging themes in DNA topoisomerase research. *Methods Mol. Biol.* **582**, 1–9
15. Papini, F. S., Seifert, M., and Dulin, D. (2019) High-yield fabrication of DNA and RNA constructs for single molecule force and torque spectroscopy experiments. *Nucleic Acids Res.* **47**, e144
16. Paik, D. H., Roskens, V. A., and Perkins, T. T. (2013) Torsionally constrained DNA for single-molecule assays: an efficient, ligation-free method. *Nucleic Acids Res.* **41**, e179
17. Gruber, S., Lof, A., Sedlak, S. M., Benoit, M., Gaub, H. E., and Lipfert, J. (2020) Designed anchoring geometries determine lifetimes of biotin-streptavidin bonds under constant load and enable ultra-stable coupling. *Nanoscale* **12**, 21131–21137
18. Sedlak, S. M., Schendel, L. C., Gaub, H. E., and Bernardi, R. C. (2020) Streptavidin/biotin: tethering geometry defines unbinding mechanics. *Sci. Adv.* **6**, eaay5999
19. Lof, A., Walker, P. U., Sedlak, S. M., Gruber, S., Obser, T., Brehm, M. A., et al. (2019) Multiplexed protein force spectroscopy reveals equilibrium protein folding dynamics and the low-force response of von Willebrand factor. *Proc. Natl. Acad. Sci. U. S. A.* **116**, 18798–18807
20. Neuert, G., Albrecht, C., Pamir, E., and Gaub, H. E. (2006) Dynamic force spectroscopy of the digoxigenin-antibody complex. *FEBS Lett.* **580**, 505–509
21. Janissen, R., Berghuis, B. A., Dulin, D., Wink, M., van Laar, T., and Dekker, N. H. (2014) Invincible DNA tethers: covalent DNA anchoring for enhanced temporal and force stability in magnetic tweezers experiments. *Nucleic Acids Res.* **42**, e137
22. Grandbois, M., Beyer, M., Rief, M., Clausen-Schaumann, H., and Gaub, H. E. (1999) How strong is a covalent bond? *Science* **283**, 1727–1730
23. Riener, C. K., Kienberger, F., Hahn, C. D., Buchinger, G. M., Egwim, I. O. C., Haselgrübler, T., et al. (2003) Heterobifunctional crosslinkers for tethering single ligand molecules to scanning probes. *Anal. Chim. Acta* **497**, 101–114
24. Zimmermann, J. L., Nicolaus, T., Neuert, G., and Blank, K. (2010) Thiol-based, site-specific and covalent immobilization of biomolecules for single-molecule experiments. *Nat. Protoc.* **5**, 975–985

ASBMB

25. Eeftens, J. M., van der Torre, J., Burnham, D. R., and Dekker, C. (2015) Copper-free click chemistry for attachment of biomolecules in magnetic tweezers. *BMC Biophys.* **8**, 9

26. Woodside, M. T., Behnke-Parks, W. M., Larizadeh, K., Travers, K., Herschlag, D., and Block, S. M. (2006) Nanomechanical measurements of the sequence-dependent folding landscapes of single nucleic acid hairpins. *Proc. Natl. Acad. Sci. U. S. A.* **103**, 6190–6195

27. Dobrovolskaia, I. V., and Arya, G. (2012) Dynamics of forced nucleosome unraveling and role of nonuniform histone-DNA interactions. *Biophys. J.* **103**, 989–998

28. Rico, F., Gonzalez, L., Casuso, I., Puig-Vidal, M., and Scheuring, S. (2013) High-speed force spectroscopy unfolds titin at the velocity of molecular dynamics simulations. *Science* **342**, 741–743

29. Herrero-Galan, E., Fuentes-Perez, M. E., Carrasco, C., Valpuesta, J. M., Carrascosa, J. L., Moreno-Herrero, F., et al. (2013) Mechanical identities of RNA and DNA double helices unveiled at the single-molecule level. *J. Am. Chem. Soc.* **135**, 122–131

30. Smith, D. E., Tans, S. J., Smith, S. B., Grimes, S., Anderson, D. L., and Bustamante, C. (2001) The bacteriophage straight phi29 portal motor can package DNA against a large internal force. *Nature* **413**, 748–752

31. Kornberg, R. D. (1974) Chromatin structure: a repeating unit of histones and DNA. *Science* **184**, 868–871

32. Richmond, T. J., and Davey, C. A. (2003) The structure of DNA in the nucleosome core. *Nature* **423**, 145–150

33. Lowary, P. T., and Widom, J. (1998) New DNA sequence rules for high affinity binding to histone octamer and sequence-directed nucleosome positioning. *J. Mol. Biol.* **276**, 19–42

34. Dyer, P. N., Edayathumangalam, R. S., White, C. L., Bao, Y., Chakravarthy, S., Muthurajan, U. M., et al. (2004) Reconstitution of nucleosome core particles from recombinant histones and DNA. *Methods Enzymol.* **375**, 23–44

35. Luger, K., Rechsteiner, T. J., and Richmond, T. J. (1999) Preparation of nucleosome core particle from recombinant histones. *Methods Enzymol.* **304**, 3–19

36. Kaczmarczyk, A., Brouwer, T. B., Pham, C., Dekker, N. H., and van Noort, J. (2018) Probing chromatin structure with magnetic tweezers. *Methods Mol. Biol.* **1814**, 297–323

37. Lo, Y. M., Mehal, W. Z., and Fleming, K. A. (1988) Rapid production of vector-free biotinylated probes using the polymerase chain reaction. *Nucleic Acids Res.* **16**, 8719

38. Lipfert, J., Hao, X., and Dekker, N. H. (2009) Quantitative modeling and optimization of magnetic tweezers. *Biophys. J.* **96**, 5040–5049

39. te Velthuis, A. J., Kerssemakers, J. W., Lipfert, J., and Dekker, N. H. (2010) Quantitative guidelines for force calibration through spectral analysis of magnetic tweezers data. *Biophys. J.* **99**, 1292–1302

40. Lipfert, J., Skinner, G. M., Keegstra, J. M., Hensgens, T., Jager, T., Dulin, D., et al. (2014) Double-stranded RNA under force and torque: similarities to and striking differences from double-stranded DNA. *Proc. Natl. Acad. Sci. U. S. A.* **111**, 15408–15413

41. van Mameren, J., Gross, P., Farge, G., Hooijman, P., Modesti, M., Falkenberg, M., et al. (2009) Unraveling the structure of DNA during overstretching by using multicolor, single-molecule fluorescence imaging. *Proc. Natl. Acad. Sci. U. S. A.* **106**, 18231–18236

42. Florin, E. L., Moy, V. T., and Gaub, H. E. (1994) Adhesion forces between individual ligand-receptor pairs. *Science* **264**, 415–417

43. Strick, T. R., Croquette, V., and Bensimon, D. (1998) Homologous pairing in stretched supercoiled DNA. *Proc. Natl. Acad. Sci. U. S. A.* **95**, 10579–10583

44. Vanderlinden, W., Skoruppa, E., Kolbeck, P., Carlon, E., and Lipfert, J. (2022) DNA fluctuations reveal the size and dynamics of topological domains. *PNAS Nexus* **1**, pgac26

45. Anderson, J. P., Angerer, B., and Loeb, L. A. (2005) Incorporation of reporter-labeled nucleotides by DNA polymerases. *Biotechniques* **38**, 257–264

46. Hoshino, H., Kasahara, Y., Fujita, H., Kuwahara, M., Morihiro, K., Tsunoda, S. I., et al. (2016) Consecutive incorporation of functionalized nucleotides with amphiphilic side chains by novel KOD polymerase mutant. *Bioorg. Med. Chem. Lett.* **26**, 530–533

47. Kuwahara, M., Nagashima, J., Hasegawa, M., Tamura, T., Kitagata, R., Hanawa, K., et al. (2006) Systematic characterization of 2'-deoxynucleoside- 5'-triphosphate analogs as substrates for DNA polymerases by polymerase chain reaction and kinetic studies on enzymatic production of modified DNA. *Nucleic Acids Res.* **34**, 5383–5394

48. Kuwahara, M., Takano, Y., Kasahara, Y., Nara, H., Ozaki, H., Sawai, H., et al. (2010) Study on suitability of KOD DNA polymerase for enzymatic production of artificial nucleic acids using base/sugar modified nucleoside triphosphates. *Molecules* **15**, 8229–8240

49. Paul, N., and Yee, J. J. B. (2010) PCR Incorporation of Modified dNTPs: The Substrate Properties of Biotinylated dNTPs. *Biotechniques* **48**, 333–334

50. Tasara, T., Angerer, B., Damond, M., Winter, H., Dörhöfer, S., Hübscher, U., et al. (2003) Incorporation of reporter molecule-labeled nucleotides by DNA polymerases. II. High-density labeling of natural DNA. *Nucleic Acids Res.* **31**, 2636–2646

51. Solis, F. J., Bash, R., Yodh, J., Lindsay, S. M., and Lohr, D. (2004) A statistical thermodynamic model applied to experimental AFM population and location data is able to quantify DNA-histone binding strength and internucleosomal interaction differences between acetylated and unacetylated nucleosomal arrays. *Biophys. J.* **87**, 3372–3387

52. Brower-Toland, B. D., Smith, C. L., Yeh, R. C., Lis, J. T., Peterson, C. L., and Wang, M. D. (2002) Mechanical disruption of individual nucleosomes reveals a reversible multistage release of DNA. *Proc. Natl. Acad. Sci. U. S. A.* **99**, 1960–1965

53. Claudet, C., Angelov, D., Bouvet, P., Dimitrov, S., and Bednar, J. (2005) Histone octamer instability under single molecule experiment conditions. *J. Biol. Chem.* **280**, 19958–19965

54. Mihardja, S., Spakowitz, A. J., Zhang, Y., and Bustamante, C. (2006) Effect of force on mononucleosomal dynamics. *Proc. Natl. Acad. Sci. U. S. A.* **103**, 15871–15876

55. Chien, F. T., and van Noort, J. (2009) 10 years of tension on chromatin: results from single molecule force spectroscopy. *Curr. Pharm. Biotechnol.* **10**, 474–485

56. Mack, A. H., Schlingman, D. J., Ilagan, R. P., Regan, L., and Mochrie, S. G. (2012) Kinetics and thermodynamics of phenotype: unwinding and rewinding the nucleosome. *J. Mol. Biol.* **423**, 687–701

57. Brower-Toland, B., Wacker, D. A., Fulbright, R. M., Lis, J. T., Kraus, W. L., and Wang, M. D. (2005) Specific contributions of histone tails and their acetylation to the mechanical stability of nucleosomes. *J. Mol. Biol.* **346**, 135–146

58. Kruithof, M., and van Noort, J. (2009) Hidden Markov analysis of nucleosome unwrapping under force. *Biophys. J.* **96**, 3708–3715

59. Sheinin, M. Y., Li, M., Soltani, M., Luger, K., and Wang, M. D. (2013) Torque modulates nucleosome stability and facilitates H2A/H2B dimer loss. *Nat. Commun.* **4**, 2579

60. Meng, H., Andresen, K., and van Noort, J. (2015) Quantitative analysis of single-molecule force spectroscopy on folded chromatin fibers. *Nucleic Acids Res.* **43**, 3578–3590

61. Kim, S. H., Vlijm, R., van der Torre, J., Dalal, Y., and Dekker, C. (2016) CENP-A and H3 nucleosomes display a similar stability to force-mediated disassembly. *PLoS One* **11**, e0165078

62. Bancaud, A., Conde e Silva, N., Barbi, M., Wagner, G., Allemand, J. F., Mozziconacci, J., et al. (2006) Structural plasticity of single chromatin fibers revealed by torsional manipulation. *Nat. Struct. Mol. Biol.* **13**, 444–450

63. Kerssemakers, J. W. J., Laura Munteanu, E., Laan, L., Noetzel, T. L., Janson, M. E., and Dogterom, M. (2006) Assembly dynamics of microtubules at molecular resolution. *Nature* **442**, 709–712

64. Mochrie, S. G., Mack, A. H., Schlingman, D. J., Collins, R., Kamenetska, M., and Regan, L. (2013) Unwinding and rewinding the nucleosome inner turn: force dependence of the kinetic rate constants. *Phys. Rev. E Stat. Nonlin Soft Matter Phys.* **87**, 012710

65. Mueller-Planitz, F., Klinker, H., Ludwigsen, J., and Becker, P. B. (2013) The ATPase domain of ISWI is an autonomous nucleosome remodeling machine. *Nat. Struct. Mol. Biol.* **20**, 82–89

66. Leger, J. F., Robert, J., Bourdieu, L., Chatenay, D., and Marko, J. F. (1998) RecA binding to a single double-stranded DNA molecule: a possible role

of DNA conformational fluctuations. *Proc. Natl. Acad. Sci. U. S. A.* **95**, 12295–12299

67. Brons-Poulsen, J., Nohr, J., and Larsen, L. K. (2002) Megaprimer method for polymerase chain reaction-mediated generation of specific mutations in DNA. *Methods Mol. Biol.* **182**, 71–76

68. Brons-Poulsen, J., Petersen, N. E., Horder, M., and Kristiansen, K. (1998) An improved PCR-based method for site directed mutagenesis using megaprimers. *Mol. Cell. Probes* **12**, 345–348

69. Krietenstein, N., Wippo, C. J., Lieleg, C., and Korber, P. (2012) Genome-wide *in vitro* reconstitution of yeast chromatin with in vivo-like nucleosome positioning. *Methods Enzymol.* **513**, 205–232

70. Walker, P. U., Vanderlinden, W., and Lipfert, J. (2018) Dynamics and energy landscape of DNA plectoneme nucleation. *Phys. Rev. E* **98**, 042412

71. Cnossen, J. P., Dulin, D., and Dekker, N. H. (2014) An optimized software framework for real-time, high-throughput tracking of spherical beads. *Rev. Sci. Instrum.* **85**, 103712

72. Konrad, S. F., Vanderlinden, W., Frederickx, W., Brouns, T., Menze, B. H., De Feyter, S., *et al.* (2021) High-throughput AFM analysis reveals unwrapping pathways of H3 and CENP-A nucleosomes. *Nanoscale* **13**, 5435–5447

73. Konrad, S. F., Vanderlinden, W., and Lipfert, J. (2021) A high-throughput pipeline to determine DNA and nucleosome conformations by AFM imaging. *Bio Protoc.* **11**, e4180

74. Bussiek, M., Mucke, N., and Langowski, J. (2003) Polylysine-coated mica can be used to observe systematic changes in the supercoiled DNA conformation by scanning force microscopy in solution. *Nucleic Acids Res.* **31**, e137

75. Vanderlinden, W., Lipfert, J., Demeulemeester, J., Debyser, Z., and De Feyter, S. (2014) Structure, mechanics, and binding mode heterogeneity of LEDGF/p75-DNA nucleoprotein complexes revealed by scanning force microscopy. *Nanoscale* **6**, 4611–4619

76. Lisitsa, T. S., Shershov, V. E., Spitsyn, M. A., Guseinov, T. O., Ikonnikova, A. Y., Fesenko, D. O., *et al.* (2017) The kinetics of fluorescent DNA labeling using PCR with different Taq polymerases depends on the chemical structures of modified nucleotides. *Biophysics* **62**, 366–372

77. Basu, S., Finke, A., Vera, L., Wang, M., and Olieric, V. (2019) Making routine native SAD a reality: lessons from beamline X06DA at the swiss light source. *Acta Crystallogr. D Struct. Biol.* **75**, 262–271